

Agile low phase noise radio-frequency sine wave generator applied to experiments on ultracold atoms

O. Morizot, J. de Lapeyre de Bellair, F. Wiotte, O. Lopez, P.-E. Pottie, and H. Perrin*
*Laboratoire de physique des lasers, Institut Galilée, Université Paris 13 and CNRS,
 Avenue J.-B. Clément, F-93430 Villetaneuse, France*

(Dated: October 31, 2018)

We report on the frequency performance of a low cost (~ 500 \$) radio-frequency sine wave generator, using direct digital synthesis (DDS) and a field-programmable gate array (FPGA). The output frequency of the device may be changed dynamically to any arbitrary value ranging from DC to 10 MHz without any phase slip. Sampling effects are substantially reduced by a high sample rate, up to 1 MHz, and by a large memory length, more than 2×10^5 samples. By using a low noise external oscillator to clock the DDS, we demonstrate a phase noise as low as that of the master clock, that is at the level of -113 dB.rad²/Hz at 1 Hz from the carrier for an output frequency of 3.75 MHz. The device is successfully used to confine an ultracold atomic cloud of rubidium 87 in a RF-based trap, and there is no extra heating from the RF source.

PACS numbers: 39.25.+k, 06.30.Ft, 07.57.Hm

I. INTRODUCTION

Radio-frequency (RF) fields are used in cold atom experiments for different purposes: for instance, evaporative cooling performed in a magnetic trap relies on RF field coupling between the different atomic magnetic states [1, 2]. This technique led to the first observation of Bose-Einstein condensation (BEC) [3, 4]. Also, RF pulses are used for dissociating ultracold molecules produced from ultracold gases through Feshbach resonances [5]. More recently, RF fields have been used together with static magnetic fields for trapping ultracold atoms at a temperature of a few μ K in unusual geometries [6, 7]. There is a growing interest for these “RF-based traps” among atomic physicists, for creating double well traps on atom chips [8, 9, 10] or proposing new kinds of confining potentials [11, 12, 13]. In both cases, a single frequency RF signal must be frequency swept over some range, often larger than the initial frequency, following a precise time function lasting several seconds. Typically the RF frequency is varied between 1 MHz and a few tens of MHz in 0.1 s to 10 s in the ramping stage, and held at the final frequency for seconds in the plateau stage. For cooling purposes, commercial RF generators fit physicists’ needs reasonably well, even if a better resolution in arbitrary frequency ramps would be appreciated. However, in the case of RF-based trapping, the requirements are stronger. The main difference between these two situations is as follows: in evaporative cooling the cold atomic sample is located away from the region of efficient coupling, whereas in the RF-based trapping scheme the atoms sit exactly at the point where the RF field has the largest effect. The quality of the RF source is then much more important than for evaporative cooling. In fact, the cloud position is directly related to the value

of the RF field frequency, and the trap restoring force, or equivalently the oscillation frequency ν_t in the harmonic approximation, is linked to the RF amplitude. As a result, any amplitude noise, frequency noise or phase noise of the RF signal during the ramp or the plateau leads to a heating of the cold atomic cloud. This motivated the construction of a synthesizer fitting our requirements.

This paper is organized as follows. In section II we give explicit expressions for the heating of the cold atom sample for frequency and amplitude noise in the case of RF-based trapping. In section III, we describe our RF synthesizer. Finally, section IV is devoted to experimental results on its performance and comparison between the different RF sources tested on the BEC experiment.

II. REQUIREMENTS ON THE RF SOURCE FOR RF-BASED TRAPPING

In this section, we will focus on the RF-dressed trap that we experimentally produce in the laboratory [7]. The extension of the main conclusions to other RF-dressed trap geometries is straightforward.

The trap confines the atoms in all three space dimensions. The trapping force arises from the interaction between the linearly polarized RF field $B(t) = B_{\text{RF}} \cos(2\pi\nu_{\text{RF}}t)$ and the atoms in the presence of an inhomogeneous magnetic field. This interaction results in a transverse confinement of the atoms to the surface of an ellipsoid. The atoms are free to move along the confining surface, resulting in a kind of “bubble trap” [6]. Due to gravity, however, the atoms are concentrated at the bottom of the ellipsoid. Their motion is pendulum-like in the horizontal directions, and imposed by the RF interaction along the vertical z axis. This last direction is thus the most sensitive to the RF field properties (frequency ν_{RF} , amplitude B_{RF}) and we will concentrate on the vertical motion in the following. Along this direction, heating or atomic losses may arise from frequency

*Electronic address: helene.perrin@galilee.univ-paris13.fr

or amplitude noise, phase hops or sudden frequency hops during the RF ramp.

A. Dipolar excitation heating

Very generally, for atoms in a one dimensional harmonic trap with a trapping frequency ν_z , any effect producing a jitter in the trap position z results in linear heating through dipolar excitation. The average energy of the cold atomic cloud E increases linearly as [14]:

$$\dot{E} = \frac{1}{4} M \omega_z^4 S_z(\nu_z) \quad (1)$$

where $\omega_z = 2\pi\nu_z$, M is the atomic mass and S_z is the one-sided Power Spectral Density (PSD) of the position fluctuations δz , defined as the Fourier transform of the time correlation function [14]

$$S_z(\nu) = 4 \int_0^\infty d\tau \cos(2\pi\nu\tau) \langle \delta z(t) \delta z(t + \tau) \rangle. \quad (2)$$

The time variations of energy, E , and temperature, T , are related by $\dot{T} = \dot{E}/3k_B$. The factor 3 arises because only one degree of freedom is responsible for the temperature increase, as is the case in our atom trap. The vertical trap position z is linked to the RF frequency ν_{RF} by $z = Z(\nu_{\text{RF}})$ such that S_z is directly proportional to S_y , the PSD of relative frequency noise of the RF source, through:

$$S_z(\nu) = \left(\nu_{\text{RF}} \frac{dZ}{d\nu_{\text{RF}}} \right)^2 S_y(\nu). \quad (3)$$

The function Z depends on the geometry of the static magnetic field. In a quadrupolar field, for instance, Z is linear with ν_{RF} and its derivative is simply a constant. From Eqs. (1) and (3), we infer that the linear heating rate is proportional to $S_y(\nu_z)$.

To fix orders of magnitude, within the static magnetic field of our Ioffe-Pritchard trap [7], ν_z may be adjusted between 600 and 1500 Hz and the typical temperature of the cold rubidium 87 atoms ranges from 0.5 to 5 μK . To maintain a temperature below condensation threshold for a few seconds, a linear temperature increase below 0.1 $\mu\text{K}/\text{s}$ is necessary. This rate corresponds to $\sqrt{S_z(\nu_z)} = 0.27 \text{ nm}/\sqrt{\text{Hz}}$ for an intermediate trap frequency of 1000 Hz and $\nu_{\text{RF}} = 3 \text{ MHz}$, which in turn corresponds to a one-sided PSD of relative frequency fluctuations of the RF source $S_y(\nu_z) = -118 \text{ dB/Hz}$.

B. Parametric heating

Fluctuations of the RF field amplitude B_{RF} are responsible for parametric heating in the vertical direction. The trapping frequency ν_z is inversely proportional to

$\sqrt{B_{\text{RF}}}$ [6]:

$$\nu_z = \left(\frac{dZ}{d\nu_{\text{RF}}} \right)^{-1} \sqrt{\frac{2F\hbar}{M\gamma B_{\text{RF}}}}. \quad (4)$$

Here, γ is the gyromagnetic ratio of the atom and F is the total atomic spin ($F = 2$ for rubidium 87 in its upper hyperfine state). The atoms are assumed to be polarized in their extreme $m_F = F$ substate. The cloud temperature increases exponentially due to amplitude noise with a rate Γ , where

$$\Gamma = \pi^2 \nu_z^2 S_a(2\nu_z) \quad (5)$$

and S_a is the PSD of the relative RF amplitude noise [14]. In order to perform experiments with the BEC within a time scale of a few seconds, Γ should not exceed 10^{-2} s^{-1} . Again, for a typical oscillation frequency of 1000 Hz, this corresponds to $S_a < -90 \text{ dB/Hz}$. This requirement is rather easy to match and does not limit the choice of the RF source, as -110 dB/Hz is commonly reached. However, particular care must be taken in the choice and installation of the RF amplifier usually used after the source.

C. Phase hops

Controlling the phase of the RF source is not a crucial point for evaporative cooling, but is an issue in the case of RF-based traps, where it is associated with trap losses. In the latter situation, the atomic spin follows an effective magnetic field oscillating at the RF frequency. A phase hop results in a sudden flip of this effective field, the atomic spin being then misaligned with the new direction of the field. Some of the atoms end up with a spin oriented incorrectly and escape the trap.

For this reason, phase hops should be avoided. This is difficult to achieve with an analog synthesizer over a wide frequency sweep. By contrast, Direct Digital Synthesis (DDS) technology is well adapted to this requirement [16].

D. Frequency steps

The drawback of DDS technology is that, although the phase is continuous, the frequency is increased by N successive discrete steps $\delta\nu$. A sudden change in the RF frequency also results in atomic losses, through the same mechanism as for phase hops. The effective magnetic field rotates, at most, by the small angle $\delta\theta = 2\pi \delta\nu / (\gamma B_{\text{RF}}/2)$ [15]. For a linear ramp over a frequency range $\Delta\nu = N\delta\nu$, the fraction of atoms remaining after the full ramp is of order $(1 - F\delta\theta^2/2)^N$. Given the expression for $\delta\theta$, this reads:

$$\left(1 - \frac{F}{2} \left(\frac{4\pi \Delta\nu}{N\gamma B_{\text{RF}}} \right)^2 \right)^N \simeq 1 - \frac{F}{2N} \left(\frac{4\pi \Delta\nu}{\gamma B_{\text{RF}}} \right)^2. \quad (6)$$

Thus, for the remaining fraction to be larger than 95%, the number of frequency steps should be larger than $10F(4\pi\Delta\nu/\gamma B_{\text{RF}})^2$. For example, for a 2 MHz ramp with a typical RF amplitude of 200 mG, N should be larger than 16,000.

In addition to this loss effect, a sudden change in the RF frequency results in a sudden shift of the position of the RF-dressed trap. This may cause dipolar heating of the atoms, especially if this frequency change occurs every trap period. The frequency steps should thus be as small as possible, a few tens Hz to a hundred Hz typically.

III. DEVICE DESCRIPTION

Our experiment has the following requirements. First, during the ramp the gap between two successive frequencies must fulfil the criterion discussed in section II D. Second, adiabaticity criteria require a controlled, optimized ramp. Third, the ramp duration should be tunable from one experiment to the other on a time scale ranging from 50 ms to 10 s. Finally, frequency and amplitude noise must be small enough, as discussed in previous section.

Given the amplitude of the frequency sweep we need to perform in our experiment, DDS technology appears to be an ideal solution. We previously used a commercial DDS-based RF generator, the Stanford DS-345. Its memory length is limited to 1,500 frequency points for each waveform with an adjustable step duration of 40 Msample/s/ N , with $N=1$ to $2^{34} - 1$. The major inconvenience of this device is that it is unable to hold the final frequency at the end of the ramp. Instead, the frequency sweep is looped indefinitely. It forced us to sacrifice either frequency resolution during the ramp or duration of the plateau. To benefit from both a low noise RF spectrum during the ramp and a very small frequency step, and to improve the possibilities of the RF source, we designed a digital RF synthesizer with a $> 200,000$ memory length and great agility, fitted to our experimental requirements.

The main features of the RF synthesizer are as follows. It is able to generate 262,144 sine waves in a row in the radio frequency band (DC - 10 MHz), owing to its 1 M-byte fast asynchronous Static Random Access Memory (SRAM). Each frequency is an integer chosen by the user. A key feature of the device is a variable sample frequency over the sequence, as the duration of each generated frequency can be tuned from 1 μ s to 1 hour.

The general architecture of the device is sketched in Fig. 1. It is made up of one evaluation kit DDS board, and a “starter kit” Field Programmable Gate Array (FPGA) board. The device is managed by a Personal Computer (PC). The DDS is clocked by an ultra-stable external reference signal. The output of the DDS is a sine wave, filtered through a 10 MHz low-pass filter. The frequency ramp synthesis starts when a TTL signal is sent to the device.

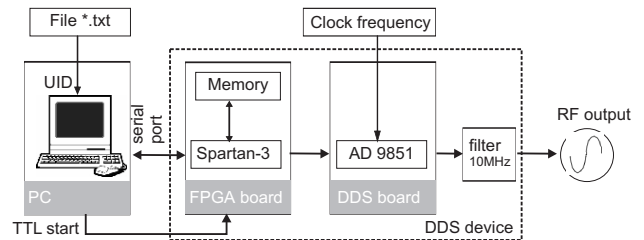


FIG. 1: Layout of the system.

The DDS board combines digital parameters and an analog reference clock frequency to generate a sine wave [16]. The heart of the DDS board is a digitally programmable device using DDS technology, the AD9851. It has a 32-bit phase accumulator, a 14-bit digital phase-to-amplitude converter and a 10-bit Digital-to-Analog Converter (DAC). Its maximum clock frequency is 180 MHz, and its maximum output frequency is 70 MHz. The phase, relative to the clock signal, is encoded in 5 bits, and is adjustable to any value from 0 to 2π . This results in a rather poor phase resolution of 196 mrad.

The FPGA board manages the 1 Mb memory, the time settings and the input/output of the device through serial port. The FPGA is a Xilinx spartan-3 XC3S200, providing 200,000 logic gates. These logic gates are designed with VHDL [17]. A Universal Asynchronous Receiver Transmitter (UART) and a Picoblaze microcontroller are loaded into the FPGA, in order to communicate through serial port to the PC and to load the on-board memory. We wrote our own VHDL scripts to manage the DDS board and the FPGA in-board memory. The FPGA board is clocked internally at 50 MHz. The output sample rate of the device depends on the number of clock cycles n_{cycle} between frequency data transferred to the DDS board. We set $n_{\text{cycle}} = 50$ so that $n_{\text{cycle}}/50 \text{ MHz} = 1 \mu\text{s}$, large enough thus ensuring safe operation of the frequency data.

Software was developed in C with CVI Labwindows in order to configure the device. The user writes a plain text file ordering all the frequencies of the desired frequency ramp. The set of frequencies is separated into 10 groups of adjustable length, with a given sample rate for each. The group lengths and the corresponding sample rate are each translated by the software into 4 bytes. In addition, each frequency in a given group, an integer written as a decimal number, is translated into 4 bytes (32 bits). The software sends these bytes by serial port to the FPGA board.

The clock frequency f_c and its phase noise level are the key points for setting the frequency performance of the device. The lower the phase noise of the clock signal, the lower is the *minimum* phase noise of the output frequency of the device (see section IV A).

The clock signal used for the experiment, see next section, is the 10 MHz clock signal from an ultra-stable Oven Controlled Crystal Oscillator (OCXO) BVA-8600.

Its phase noise PSD is -115 dB.rad²/Hz at 1 Hz. As this clock frequency is very close to the desired maximum output frequency ($\simeq 10$ MHz, see next section), and to fulfil Shannon’s theorem [18, 19], we generate a higher clock frequency by using the internal frequency clock multiplier, at $\times 6$, of the DDS board.

IV. RESULTS

The device presented in section III was first tested for its frequency stability performance, as described in section IV A and summarized in Table I. It was then integrated into a Bose-Einstein condensation experiment, see section IV B.

A. Device frequency performance

1. Quantization error, Phase Accumulator truncation and “magic” frequencies

By construction, digitization yields to inaccuracies in frequency synthesis. The output frequency of 32-bit resolution DDS is given by

$$f_{RF} = f_c \times \frac{w}{2^{32}} \quad (7)$$

where w is a binary 32-bit tuning word. The output frequency can thus differ slightly from the desired frequency. As $f_c = 60$ MHz, the maximum digitization error δf is $6 \times 10^7 / 2^{32} = 0.014$ Hz.

As our software only takes integer frequencies as input, a given frequency f_{RF} will be synthesized without sampling error if it may be written exactly as an integer in the form given at Eq. (7). This condition is written as:

$$w = n \times 2^{32-p} \quad (8)$$

where n is a positive integer and p is the power of 2 in the prime factorization of the clock frequency f_c . In our case, $f_c = 2^8 \times 3 \times 5^7$ Hz and $p = 8$ so that every frequency verifying

$$f_{RF} = n \times 234375 \text{ Hz} \quad (9)$$

will yield to no digitization error. n should be less than $2^p/3$ for the desired frequency to be in the synthesizer range ($f_c/3$).

In addition, when the AD9851 converts the calculated phase to an effective output amplitude, only the first most significant 14 bits are used, even though the AD9851 is a 32-bit synthesizer, in order to handle practicable number of entries in a lookup table. Truncating the phase results in errors in amplitude that are periodic in the time domain. These errors will be seen as spurs in the frequency domain. However, for particular frequencies which are exactly encoded by the first 14 bits (The

TABLE I: Performance of the device with $f_c = 60$ MHz. The relative frequency noise is computed from the phase noise data, and given for 3.75 MHz (“magic” frequency) and 3 MHz (larger noise value).

Parameters	Min.	Max.	Units
Dynamic	0	10	MHz
Line-width	-	30	mHz
Digitalization error	0	14	mHz
Sample rate	adjustable	1	MHz
Memory length	1	262,144	pts
Phase noise@1Hz	-113	-78	dB.rad ² /Hz
Rel. freq. noise@1Hz	-244	-207	dB/Hz
Rel. ampl. noise@1Hz	-	-120	dB/Hz

last 18 bits are 0.), the phase is not truncated at all, yielding no spurious effects and the best PSD of phase noise. This occurs for every frequency satisfying

$$f_{RF} = n \times f_c / 2^{14} \quad (10)$$

with n a positive integer. As $f_c = 60$ MHz, we have $f_{RF} = n \times 3662.109375$ Hz. The most stringent condition being the first one, we will denote the frequencies satisfying Eq. (9) as “magic frequencies”. In order to illustrate the difference between a “magic frequency” and another one, we performed a set of noise PSD measurements for two frequencies: a first set for $f_{RF} = 3$ MHz which is not a “magic” frequency, and a second set for $f_{RF} = 3.75$ MHz which is a “magic” frequency.

2. Spectral density of noise

We recorded the spectral density of noise of our synthesizer at a given frequency f_{RF} by FFT analysis of the beat note at 0 Hz with a second synthesized reference signal. The measurement bench is sketched in Fig. 2. In order to generate a tunable reference signal in the RF range we used an analog synthesizer, Rhode & Schwartz SML-01 (R&S), for synthesizing a signal at a high frequency, and then divided by 100 to give f_{RF} for subsequent mixing. The beat note was recorded and analyzed by a digital FFT analyzer HP 3562A sampling at 256 kHz. The R&S, as all the measurement devices, was clocked at 10 MHz by the ultra-stable BVA-8600 quartz oscillator. All the plots shown on Fig. 3 are raw spectra of the beat note. The reference signal (R&S) itself was characterized by making a beat note with a second identical R&S based synthesis. This corresponds to the line labelled as “Reference” in Fig. 3.

By tuning the phase difference ϕ between the RF signal and the reference signal to $\pi/2$, we recorded phase noise. At $f_{RF} = 3$ MHz, the PSD of phase noise is -78 dB.rad².Hz⁻¹ at 1 Hz, which corresponds to a PSD of relative frequency noise of -207 dB.Hz⁻¹. From the

data reported on Fig. 3, and assuming a Lorentzian line-shape for the beat note, the linewidth δf of the RF signal, given by

$$\delta f = \pi \nu_{RF}^2 \frac{1}{\Delta f} \int_{\Delta f} df S_y(f), \quad (11)$$

is as small as 30 mHz over a bandwidth $\Delta f = 100$ kHz for an output frequency of 3 MHz [23]. We found similar results for output frequencies from 1 to 5 MHz. At a “magic” frequency, as for example at 3.75 MHz, where truncation effects cancel out, the results are even better, with a PSD of phase noise as low as -113 dB.rad².Hz⁻¹ at 1 Hz, only 2 dB higher than the phase noise of the BVA 8600. The observed value corresponds to the ultimate phase noise of the DDS chip specified by the manufacturer. The relative frequency noise is then -244 dB.Hz⁻¹.

The frequency noise performance is naturally linked to the quality of the master oscillator. To illustrate this fact, the same measurements were repeated with the improved OCXO of a DS-345, the ERC EROS-750-SBR-4, as master oscillator. No significant change in the frequency performances were noticed at non magic frequencies. At a magic frequency, the PSD of phase noise increased to -100 dB.rad²/Hz, which is consistent with the phase noise specifications of this quartz.

The PSD of relative amplitude noise S_a was recorded with the same measurement bench, by tuning the phase ϕ to 0. The reference signal was also delivered by the R&S. The recorded spectrum is very close to the “Reference” line itself at the level of -120 dB.Hz⁻¹ at 1 Hz, close to the input noise of the FFT analyzer. Note that for relevant excitation frequencies $\nu = 2\nu_z$ (larger than 1.2 kHz), the PSD of amplitude noise is lower than -130 dB.

In practice, we use in our BEC experiment a programmable RF attenuator Minicircuit ZAS-3, driven by an analog output channel of a National Instrument PC card PCI-6713, in order to vary the RF amplitude sent to the RF coil. We repeated the measurements described above with this attenuator and found an increase of S_a , starting at -115 dB.Hz⁻¹ at 1 Hz, which corresponds to a noise figure of the programmable attenuator of 5.1 dB. At the output of the attenuator, the RF signal is amplified by a class-A amplifier Kalmus 505 F. Its gain is

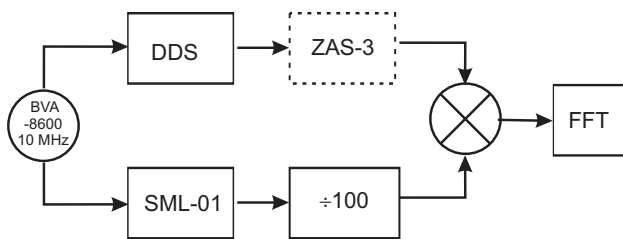


FIG. 2: Noise spectrum measurement bench. The gain in the mixer was fitted to the output signal, depending on the phase between the two beating signals.

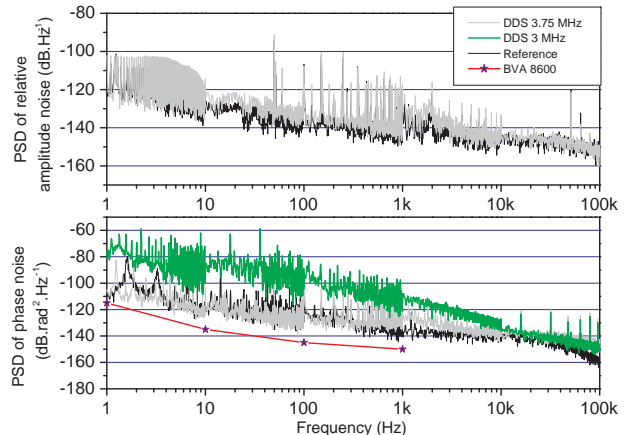


FIG. 3: PSD of relative amplitude noise, upper plot, and phase noise, lower plot. Averaging = 100. FFT’s sampling frequency = 256 kHz. The low pass filter cutting frequency of the mixer was set to 200 kHz. The reference curve corresponds to the beat note of two identical R&S synthesizers. Plotted for comparison is the phase noise specifications of the BVA 8600 quartz oscillator, as given by the manufacturer.

37 dB and its noise figure is typically +10 dB according to the manufacturer specifications.

B. Integration into the experiment

In this section, we present the main experimental results concerning the heating rate of the atomic sample.

As described in section II, the RF signal is used for producing the bubble-like trap, where ultracold rubidium atoms are accumulated at the bottom of the surface. The trap is very anisotropic with stronger confinement in the vertical direction [7]. For the RF-dressed trap to be efficiently loaded from the standard Ioffe-Pritchard static magnetic trap, described in [20], the RF frequency f_{RF} has to be ramped up from 1 MHz to a final fixed frequency f_{RF}^{end} ranging from 2 to 10 MHz. The static magnetic field, necessary both for magnetic trapping and RF-induced trapping, is always present. A typical ramp is shown on Fig. 4. The frequency is ramped more slowly around 1.3 MHz, corresponding to the resonant frequency at the center of the magnetic trap where adiabaticity of spin rotation is more difficult to obtain. At the end of this ramp, which may last between 75 ms and 500 ms, the RF frequency is held between 0.1 and 10 s for testing the lifetime and heating rate of the atoms in the RF-based trap.

The RF signal is amplified by 37 dB with a single stage amplifier, and the RF field is produced by a small circular antenna. The RF field is linearly polarized and its amplitude B_{RF} may be adjusted between 70 and 700 mG. We

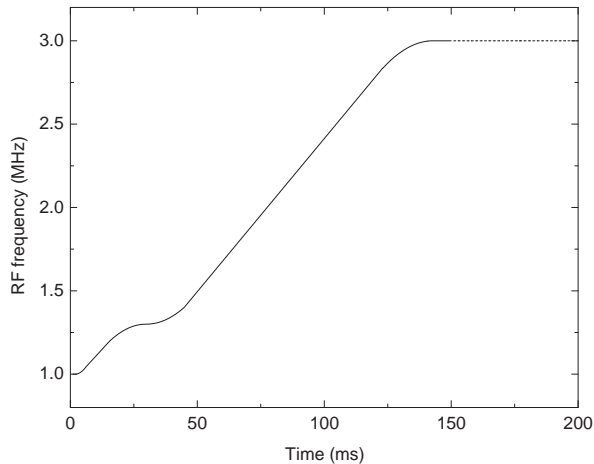


FIG. 4: Typical shape of a radio-frequency ramp applied to the ultracold atomic sample. In the present example f_{RF} is increased from 1 to 3 MHz within 150 ms. At the end of this ramp, the RF frequency is maintained at its final value for some holding time in the RF-based trap, dashed line.

record the atomic temperature after the RF ramp as a function of time while the atoms are confined in the RF-based trap. The temperature is deduced from the cloud size along z after a 7 ms of ballistic expansion. The same measurement was repeated with different RF sources.

First, we used a Agilent 33250A synthesizer with a RF amplitude larger than 500 mG for both the frequency ramp and the final holding frequency. Such RF analog synthesizers operated at fixed frequency exhibit very good relative frequency noise in most cases, typically at the -180 dB/Hz level or better. However, as mentioned by Colombe *et al.* [7] and confirmed by White *et al.* [21], the relative frequency noise increases by a few decades if the output frequency is driven with an external analog voltage. The frequency was indeed tuned through an external voltage control provided by the PC analog board (NI 6713), such that the modulation depth was ± 1 MHz on a central frequency of 2 MHz. We obtained both a short lifetime, typically 400 ms at $1/e$, and a strong linear heating, as shown on Fig. 5 full circles. The heating rate is measured to be $5.0 \mu\text{K/s}$. This rate, given the RF amplitude, corresponds to a relative frequency noise of $S_y = -100$ dB/Hz at the trap frequency of 600 Hz. This noise is quite high and is related to voltage noise on the external frequency control of the synthesizer. This effect is strong in our case as the frequency is varied with a large modulation depth ($\Delta f/f = 1$).

We also tested a two step scheme, with a first ramp performed by a Stanford DS-345 DDS (1,500 frequency points), followed by the R&S maintained at fixed frequency for the full holding time. This scheme allows one to benefit from the excellent frequency stability of the second device used at fixed frequency. With this setup,

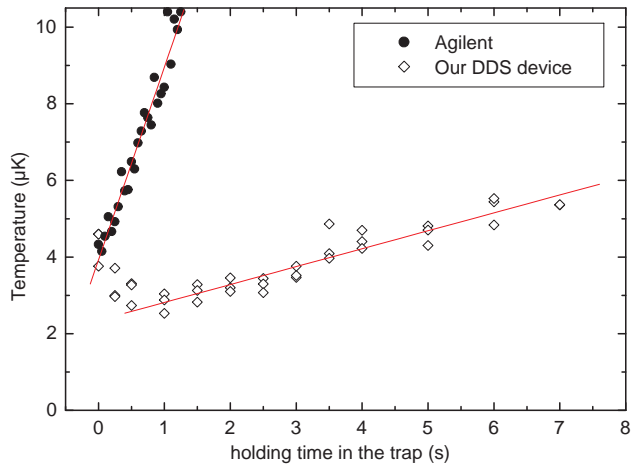


FIG. 5: Comparison of heating of the atomic cloud in the bubble trap: Agilent 33250A synthesizer, full circles, or present device, open diamonds, is used for creating the RF ramp and the final radio-frequency f_{RF}^{end} . We observe a heating rate of $5.0 \mu\text{K/s}$ in the first case and $0.47 \mu\text{K/s}$ the second one, as given by a linear fit, full lines.

heating during the plateau stage seemed to be completely suppressed [7]. However, a large dispersion was observed in the atom number data after the switching, which prevented us from characterizing the heating very precisely. This dispersion is due to a random phase hop at the switching time between the two synthesizers, resulting in atomic losses. We studied the effect of the random phase hop on the atom number by recording, for each experiment, the phase difference at the switching time with a control oscilloscope. The results are presented on Fig. 6, full circles. For the maximum phase hop, π , 80% of the atoms are lost. This figure depends on the atomic temperature, the losses being higher at lower temperature, and is well reproduced by theory, as shown on Fig. 6, black line. The theoretical curve is calculated for an RF amplitude of 470 mG by averaging the loss probability over the positions of the atoms, as deduced from a thermal distribution at a temperature of $4 \mu\text{K}$. The fact that the trap is able to hold two of the five spin components of the $F = 2$ hyperfine state is taken into account.

Finally, we performed the heating rate and lifetime measurements with our DDS device and an amplitude of 70 mG. We found an increased lifetime, up to 9.6 s. During the first second, the vertical “kinetic temperature”, deduced from the vertical cloud size after time of flight, decreases due to thermalization with the horizontal degrees of freedom which initially have a lower energy due to the loading procedure: Fig. 5, open diamonds. After 1 second, a linear heating rate of $0.47 \mu\text{K}\cdot\text{s}^{-1}$ is clearly observable. No exponential parametric heating is measurable. We believe that the remaining linear heating is due to residual excitation by scattered light, which was not present in the previous case. The same heating

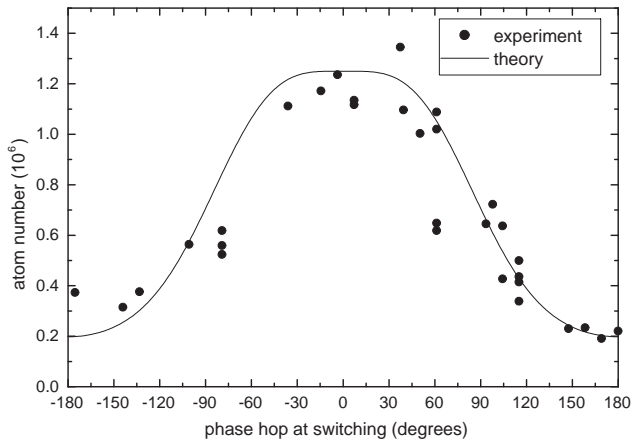


FIG. 6: Number of atoms remaining after switching between the two synthesizers as a function of the phase hop. Experimental data, full circles, are compared to a calculation, full line, assuming a RF amplitude of 470 mG and a temperature of 4 μ K.

rate was indeed observed within the static magnetic trap, when the RF source was off. Heating directly linked to the RF source is not observable.

V. CONCLUSION

We built a low cost DDS RF generator, based on a DDS chip and its evaluation kit. It is extremely agile since we have the ability of using up to 10 different time steps during the sequence, allowing an efficient use of the FPGA on-board memory. In contrast to Stanford DS-345 RF synthesizers, the frequency ramp is not repeated at the end of the sequence. The last frequency is kept until a new TTL pulse is proceeded to end the sequence. Its large memory length, up to 262,144 frequency samples, allows very small frequency steps, thus strongly reducing the atomic losses in our RF-dressed trap experiment. The DDS technology ensures that the phase is continuous all over the frequency ramp, which is essential for RF trapping applications.

Apart from these high resolution features, the device presents excellent spectral properties. The power spectral density of phase noise is as low as $-113 \text{ dB}\cdot\text{rad}^2\cdot\text{Hz}^{-1}$ at well chosen “magic frequencies”, and in any case remains below than $-78 \text{ dB}\cdot\text{rad}^2\cdot\text{Hz}^{-1}$ at worst, dominated by phase truncation. This last value yields a linewidth of 30 mHz over a 100 kHz bandwidth. The corresponding relative frequency noise level is 90 dB below the requirements of our RF-dressed trapping experiment.

The amplitude noise of the DDS synthesizer is measured to be below $-130 \text{ dB}\cdot\text{Hz}^{-1}$ at frequencies above 1 kHz. Amplitude noise turns out to be the limiting noise present in our RF chain at the present time due to the

several dB noise figures of the attenuators and amplifiers in use in our experiment. They actually increase the RF amplitude noise to $-115 \text{ dB}\cdot\text{Hz}^{-1}$ at 1 kHz, which still remains 25 dB below our experiment requirements.

All these features make our DDS apparatus very well-suited for cold atom experiments. It may be used for optimized evaporative cooling implementation, with arbitrary frequency ramp profiles including a final “RF-knife”, in a standard BEC experiment. It is of particular importance in the case of atom chip experiments [22], where the cooling ramp is usually done very quickly (1 s typically). It is also ideal for developing new RF-based traps. In particular, the possibility of configuring the time step, that is the duration of each frequency point, is very attractive for our application. This feature is all the more interesting in that the memory can be separated in several zones, each being allocated a chosen number of points and a chosen time step, so we can dilate or compress in time the whole or a part of the ramp, while keeping the same frequency series. For instance, if we want to accomplish a ramp of N frequency values with a small time resolution, say 10 μ s, and then keep the final frequency constant over ten seconds, we have the ability to address a first memory zone with the first $N - 1$ points and a 10 μ s time step, and a second memory zone with the last frequency value and a 10 s time step. A single time step over the whole sequence would have forced us to sacrifice either the resolution of the ramp or the duration of the final plateau.

The device was successfully implemented in our ultracold atom experiment. First, we set boundary specifications on the RF source performances for trapping experiments regarding heating rate and lifetime. In the same manner, we set conditions on maximum phase hops and frequency step magnitude. With our home made device, we observed no heating due to the RF source during the plateau step. A remaining heating rate of $0.47 \mu\text{K}/\text{s}$ was identical to the one obtained in the magnetic trap and was limited by other noise sources, presumably scattered photons. Despite the very large number of frequency points, heating along the vertical axis is still present during the loading stage of the RF-dressed trap. We attribute this heating to non-adiabatic deformation of the confining potential during the loading process, which we could not make slower due to the other noise sources.

While the actual performances of the device are already very good, a few improvements are still possible. First, the memory length of the DDS is basically determined by the FPGA in-board memory size. A larger sample size may easily be implemented by replacing the board, provided that the data transfer rate is improved through the use of an Ethernet port or a USB port. Second, the sample rate is 1 MHz, limited by the data transfer rate from the FPGA board. Higher FPGA clock frequency, or smaller clock counts n_{cycle} , would allow higher sample rates. The frequency limit due to the AD-9851 DDS chip itself is 3 MHz. This modification would improve the temporal resolution by a factor of 3. Finally,

the maximum output frequency of 10 MHz may be very easily increased to 20 MHz by replacing the low-pass filter. By clocking the DDS with a 180 MHz clock, one could even reach output frequencies up to 60 MHz. Note that with a similar DDS chip, the AD 9858, frequency clocks as high as 1 GHz are allowed, which makes possible the synthesis of RF frequencies up to 330 MHz.

Acknowledgments

We are indebted to R. J. Butcher for a critical reading of the manuscript. This work was supported by the

Région Ile-de-France (contract number E1213) and by the European Community through the Research Training Network “FASTNet” under contract No. HPRN-CT-2002-00304 and Marie Curie Training Network “Atom Chips” under contract No. MRTN-CT-2003-505032. Laboratoire de physique des lasers is UMR 7538 of CNRS and Paris 13 University. The LPL is a member of the Institut Francilien de Recherche sur les Atomes Froids.

-
- [1] H. F. Hess, Phys. Rev. B **34**, 3476 (1986).
 - [2] N. Masuhara, J. M. Doyle, J. C. Sandberg, D. Kleppner, T. J. Greytak, H. F. Hess, and G. P. Kochanski, Phys. Rev. Lett. **61**, 935 (1988).
 - [3] E. A. Cornell and C. E. Wieman, Rev. Mod. Phys. **74**, 875 (2002).
 - [4] W. Ketterle, Rev. Mod. Phys. **74**, 1131 (2002).
 - [5] C. A. Regal, C. Ticknor, J. L. Bohn, and D. S. Jin, Nature **424**, 47 (2003).
 - [6] O. Zobay and B. M. Garraway, Phys. Rev. Lett. **86**, 1195 (2001).
 - [7] Y. Colombe, E. Knyazchyan, O. Morizot, B. Mercier, V. Lorent, and H. Perrin, Europhys. Lett. **67**, 593 (2004).
 - [8] T. Schumm, S. Hofferberth, L. M. Andersson, S. Wildermuth, S. Groth, I. Bar-Joseph, J. Schmiedmayer, and P. Krüger, Nature Physics **1**, 57 (2005).
 - [9] M. H. T. Extavour, L. J. Le Blanc, T. Schumm, B. Cieslak, S. Myrskog, A. Stummer, S. Aubin, and J. H. Thywissen, *Proceedings of the International Conference on Atomic Physics*, Atomic Physics **20**, 241 (2006).
 - [10] G.-B. Jo, Y. Shin, T. A. Pasquini, M. Saba, W. Ketterle, and D. E. Pritchard, M. Vengalattore, and M. Prentiss, Phys. Rev. Lett. **98**, 030407 (2007).
 - [11] I. Lesanovsky, T. Schumm, S. Hofferberth, L. M. Andersson, P. Krüger, and J. Schmiedmayer, Phys. Rev. A **73**, 033619 (2006).
 - [12] Ph. W. Courteille, B. Deh, J. Fortàgh, A. Günther, S. Kraft, C. Marzok, S. Slama, and C. Zimmermann, J. Phys. B: At. Mol. Opt. Phys. **39**, 1055 (2006).
 - [13] O. Morizot, Y. Colombe, V. Lorent, H. Perrin, and B. M. Garraway, Phys. Rev. A **74**, 023617 (2006).
 - [14] M. E. Gehm, K. M. O’Hara, T. A. Savard, and J. E. Thomas, Phys. Rev. A **58**, 3914 (1998).
 - [15] The factor $B_{\text{RF}}/2$ arises from the fact that only half of the power of the linearly polarized RF has an effect on the atoms.
 - [16] B.-G. Goldberg, *Digital Techniques in Frequency Synthesis*, (Mac Graw-Hill, New-York, 1996).
 - [17] Very High Speed Integration Circuit Hardware Description Language.
 - [18] H. Nyquist, Trans. AIEE **47**, 617 (1928); reprint as classic paper in: Proc. IEEE, **90**, 280 (2002).
 - [19] C. E. Shannon, Proc. Institute of Radio Engineers **37**, 10 (1949); reprint as classic paper in: Proc. IEEE, **86**, 447 (1998).
 - [20] Y. Colombe, D. Kadio, M. Olshani, B. Mercier, V. Lorent, and H. Perrin, J. of Opt. B: Quantum Semiclass. Opt. **5**, S155 (2003).
 - [21] M. White, H. Gao, M. Pasienski, and B. DeMarco, Phys. Rev. A **74**, 023616 (2006).
 - [22] R. Folman, P. Krüger, J. Schmiedmayer, J. Denschlag, and C. Henkel, Adv. At. Mol. Opt. Phys. **48**, 263 (2002).
 - [23] D. Halford, Frequency Standards Metrology Seminar, 431-466 (1971).